# Ultra-lightweight, highly permeable, and waterproof fibrous organic electrochemical transistors for on-skin bioelectronics

Chen, Shuai; Hou, Kunqi; Li, Ting; Wu, Xihu; Wang, Zhe; Wei, Lei; Leong, Wei Lin

2022

Chen, S., Hou, K., Li, T., Wu, X., Wang, Z., Wei, L. & Leong, W. L. (2022). Ultra-lightweight, highly permeable, and waterproof fibrous organic electrochemical transistors for on-skin bioelectronics. Advanced Materials Technologies.
https://dx.doi.org/10.1002/admt.202200611

https://hdl.handle.net/10356/160305

https://doi.org/10.1002/admt.202200611

# Ultra-lightweight, Highly Permeable and Waterproof Fibrous Organic Electrochemical Transistors for On-skin Bioelectronics

*Shuai Chen, Kunqi Hou, Ting Li, Xihu Wu, Zhe Wang, Lei Wei, Wei Lin Leong**

School of Electrical and Electronic Engineering, Nanyang Technological University, 50 Nanyang Avenue, Singapore 639798, Singapore
Email: wlleong@ntu.edu.sg

Recently emerged on-skin electronics with applications in human-machine interfaces and on-body healthy monitoring call for the development of high-performance skin-like electrodes and semiconducting polymers. The development of waterproof and breathable membranes that can provide a high level of protection for human skins and a comfortable contact between electronics and skin are the pressing demands for on-skin electronics. However, major challenges remain, such as the limited mechanical durability and permeability of gas and liquid, hindering long-term stability and reusability. Herein, we report a fibrous electrolyte containing polymer matrix and ionic liquid, which is highly robust, breathable, waterproof, and conformal with human skin. Serving as fibrous substrate and electrolyte of organic electrochemical transistors (OECTs), a high transconductance of ~0.8 mS, stability over pulsing and time (~1000 cycles and 30 days) were achieved. The softness of fibrous OECTs enables a comfortable contact after attaching to human skin, which can reduce the interfacial impedance to achieve a high-quality local amplification of the electrocardiography signals (signal-to-noise ratio of 21.7 dB) even in skin squeezed state or after one week. These results indicated that our fibrous OECTs have huge potential for versatile on-skin electronics such as non-invasive medical monitoring, soft sensors, and textile electronics.

## Introduction

The emerging on-skin electronics, including wearable sensors, textile electronics, and electronic skins, have entered our daily life in recent years.[1-3] With the development of advanced materials and nanotechnology, on-skin electronics have become progressively softer and thinner, along with more attention on the breathable and waterproof behaviors of on-skin devices.[4-6] The soft and thin electronics guarantee a conformable contact with skin, enabling the withstand of bending and extreme deformation, without diminishing the integrity and functionality. Another important factor is the breathability and waterproofness of the device which can protect human skin from skin's inflammation, redness, or itch over a long time while wearing directly on the skin.[7, 8] However, most of the reported on-skin devices are thin film-based and with poor gas permeability, which do not allow free evaporation of perspiration. Wearable electronic textiles present great potential for breathable electronics on skin, weaving functional fibers together, or printing functional elements onto textile or cloths.[9-11] Although excellent breathability can be achieved for textile electronics, long-term stability, waterproofness, and skin comfortability are still considerable challenges for functional textile fabrics.

One class of devices that has received much attention in bioelectronic and wearable electronic applications is the organic electrochemical transistors (OECTs).[12-14] In an OECT, the conjugated polymer channel is in direct contact with an electrolyte which is the source of ions.[12, 13] Ionic electrochemical doping throughout the volume of conjugated polymers endows OECTs with excellent amplification capability and efficient ion-to-electron transduction at low operating voltage. Due to the operation in electrolyte solutions with a low operating voltage, OECTs are promising for biological sensing.[15, 16] OECT on Nylon fibers was reported with high sensitivity and selectivity as wearable and stretchable fabric biosensors.[17] The high transconductance ($g_m$) makes OECTs well suited to detect and amplify small electrophysiological signals (~10 μV to 10 mV) such as electrocardiography (ECG), electrooculography (EOG), electroencephalography

(EEG), and electromyography (EMG) from the skin.[18-20]

In many of the on-skin electronics and energy devices, the use of solid and quasi-solid polymer electrolytes is generally more preferred than aqueous and ionic liquid electrolytes as they can address the concerns of safety, low electrochemical stability window due to water electrolysis and potential leakage issues, limiting the long-term operation and reproducibility. However, OECTs typically utilize liquid electrolytes for fast ion transport into the conjugated polymer channel.[21-23] There are only few recent reports on the use of solid electrolytes in OECTs, such as hydrogels and ion-gels which incorporate aqueous electrolytes, or ionic liquid within an organic matrix.[24-27] However, such quasi-solid-state electrolytes can be susceptible to short operational life and viscous problem due to the water loss and poor miscibility.[28, 29] A recent report on the development of an ultrathin solid-state OECT (~ 6 um) to improve the comfort level for the skin surface when in contact with the OECT showed good operation on dry biological surfaces for long-term ECG monitoring with high signal-to-noise (~24dB).[30] This ultra-thin solid-state OECT utilized glycerol gel electrolyte and parylene film as the substrate. However, the fabrication process requires UV irradiation to tune the surface property as the coating of the ultra-thin glycerol gel electrolyte on the hydrophobic parylene layer is challenging and leads to degradation of the channel.

The blend of poly(vinylidene fluoride-co-hexafluoropropylene) (PVDF-co-HFP) ionic conductive polymer and ionic liquid, 1-ethyl-3-methylimidazolium bis(trifluoromethylsulfonyl)amide ([EMIM][TFSI] is another promising polymer electrolyte and has long drawn significant interest in organic field-effect transistors[31-34], thermoelectric generators[35, 36] and touch sensors[37-39] due to its high ionic conductivity, high polarity, high dielectric constant, wide electrochemical stability window and good thermal and mechanical stability. PVDF-co-HFP/[EMIM][TFSI] has also recently been utilized successfully in OECTs,[25, 26, 32] and revealed efficient ion transport, achieving high transconductance (~7 mS/μm), and fast transient response (~3.87 ms)[39]. However, these elastomeric

ion gels are typically too thick to be used in wearable sensors applications. Therefore, it is challenging to use these ion gels based OECTs to establish conformal contact between device and skin surface and has not yet been implemented for on-skin electronics. In addition, the waterproofness and gas permeability of solid-state OECTs are also great challenges for on-skin electronics.

In this work, we report a fibrous based OECT that is highly air-permeable and waterproof for on-skin electronics. An interconnected three-dimensional fibrous network of PVDF-co-HFP/[EMIM][TFSI] is formed by electrospinning, serving as a supporting scaffold/substrate and electrolyte simultaneously. The fibrous and porous polymer electrolyte can enable faster ion mobility and promotes better interfacial contact with the polymer channel for better ion uptake and electrochemical performance. The mechanical robustness of the fibrous electrolyte substrate was reinforced with an additional parylene coating which improves the connection between the fibers. The fabricated OECTs on fibrous electrolyte substrate were demonstrated to be lightweight (0.25 g $cm^{-2}$), insusceptible to bending deformation, operated well underwater, and showed excellent stability over ~1000 cycling times and over one-month period time. The porous structure of fibrous network also allows the free evaporation of perspiration that can be directly laminated onto human skin for high-quality electrophysiology signal recording for long-term usage. Finally, our fibrous OECT was used to record ECG signal by combining the fibrous electrode on the skin to collect the potential generated by cardiac activity and simultaneously achieve local amplification, in which a high signal-to-noise ratio of 21.7 dB was obtained. The fibrous OECT maintained its stable properties even after skin squeezing, with minor fluctuation and stable recording over time, paving the way for other electrophysiological signals as epidermal electronics.

## Results

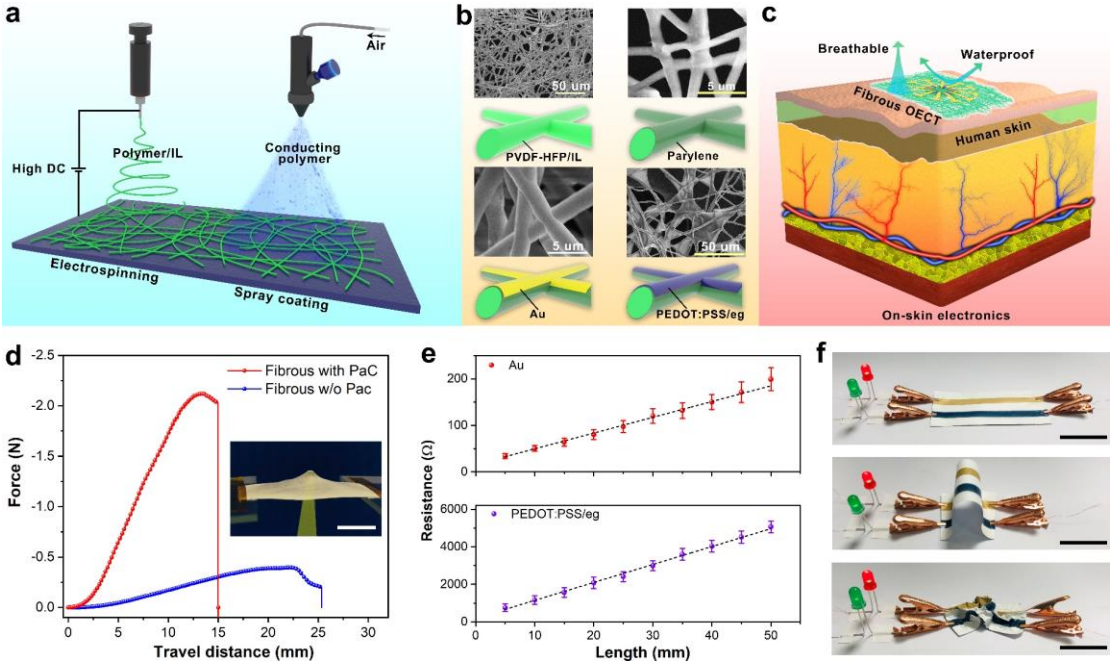


**Figure 1. Fibrous electrolyte. a** Illustration of the electrospinning and spray printing process of waterproof and breathable fibrous electrolyte. **b** Schematic and SEM images of electrospun PVDF-HFP/EMIMTFSI fibers, fibers after parylene coated, fibers after Au evaporated, and fibers after PEDOT/PSS coated. **c** A fibrous membrane on human skin as on-skin electronics with waterproof and breathable capabilities. **d** The mechanical behaviors of fibrous membrane before and after parylene coated during poking deformation. **e** The conductivities of PEDOT:PSS and Au layer on fibrous substrate. **f** The high conductivity of fibrous PEDOT:PSS and Au layer while suffering bending and twisting deformation.

**Fabrication of fibrous electrolyte.** The porous fibrous electrolyte was first synthesized by randomly distributed blend polymer/ionic-liquid fibers through a simple electrospinning process, as shown in **Fig. 1a**. Electrospinning is considered as the most effective method for fabricating continuous fibers with diameters ranging from nanometers to micrometers. Here, the fibrous electrolyte comprising PVDF-HFP as the ionic conducting polymer matrix and [EMIM][TFSI] as the ionic source was developed for on-skin electronics. The incorporation of the fluorinated polymer matrix and IL induces a high ion-dipole electrostatic interaction, thus forming a hydrophobic ionic elastomer that allows for facile ion migration. As shown in **Fig. 1b**,

the diameter of PVDF-HFP/[EMIM][TFSI] fibers are distributed in the range of 1-3 um with an average of 1.7 um. Increasing the ionic concentration induces morphology change and sparse fibers network, affecting the form of fibrous devices (Supplementary Fig. S1). Then a 300 nm-thick parylene-C (PaC) was coated through chemical vapor deposition around the surface of fibrous electrolyte to improve the continuous bonding between the fibers. **Fig. 1b** indicated the porous structure was retained after PaC was coated. Supplementary Fig. S2 showed a slightly increased fiber diameter after 300 nm PaC coating. The stress-strain curves (Supplementary Fig. S3) proved an improved mechanical behavior, where the tensile forces of the fibrous electrolyte before and after PaC coating were 20 mN and 210 mN at a tensile strain of 10%, respectively. In addition, when using a sharp tip to poke the fibrous membrane, the stress at rupture increases with the PaC layer coating, demonstrating the enhanced mechanical robustness (**Fig. 1d**). The cross-section SEM image shows an ultrathin fibrous structure with a thickness of ~8 um, allowing its high flexibility and softness, and enabling its conformable lamination and non-foreign-body-sensation on the surface of human skin (Supplementary Fig. S4). Due to its porous structure and hydrophobicity, the fibrous electronics are well-suitable for the application in breathable and waterproof on-skin electronics.

To further validate the robustness of fibrous electrolyte and feasibility as fibrous substrate, we deposited gold (Au) electrode and spray-coated PEDOT:PSS layer on the fibrous membrane. As shown in **Fig. 1b**, PaC layer helps connect the junctions between the neighboring fibers, thus improving the conductivity of deposited electrodes and conducting polymers. The PaC layer is biocompatible and can protect against chemical, moisture, and body fluids. The electrode and channel part are still in porous structures, as revealed in SEM images of Fig. 1b (bottom). The enlarged SEM image of PEDOT:PSS on fibers presented that most fibers of the electrolyte are coated with PEDOT:PSS to form the porous structure. At the same time, a few gaps between fibers are filled with freestanding PEDOT:PSS. The fibrous electrolyte with PaC is suitable as a substrate for electronics, such as to support the electrodes and conducting

polymers. The sheet resistance of Au and PEDOT:PSS on fibrous membrane were obtained to be ~ 41.56 Ω/square (3.38 Ω/mm) and 596.91 Ω/square (95.58 Ω/mm), respectively, which is much higher than that before PaC coating and comparable with that on PaC substrate (Supplementary Fig. S5). A uniform deposition can be observed from **Fig. 1e**, where shows a linear relationship between the conductivity and length. To investigate its mechanical durability under significant deformation, a fibrous membrane with coated parallel Au and PEDOT:PSS lines (W×L: 0.3 cm × 5 cm), as parts of the electric circuit, were bonded with two commercial LEDs, which allowed the LEDs to turn on at 2V bias. After bending and crumpling, the lighted LED exhibited negligible variation, demonstrating the high conductivity of the Au electrode, and PEDOT:PSS layer is maintained (**Fig. 1f**). Besides, the fibrous membrane is found to retain its conductivity after unfolded deformation and bending at different angles (Supplementary Fig. S6).

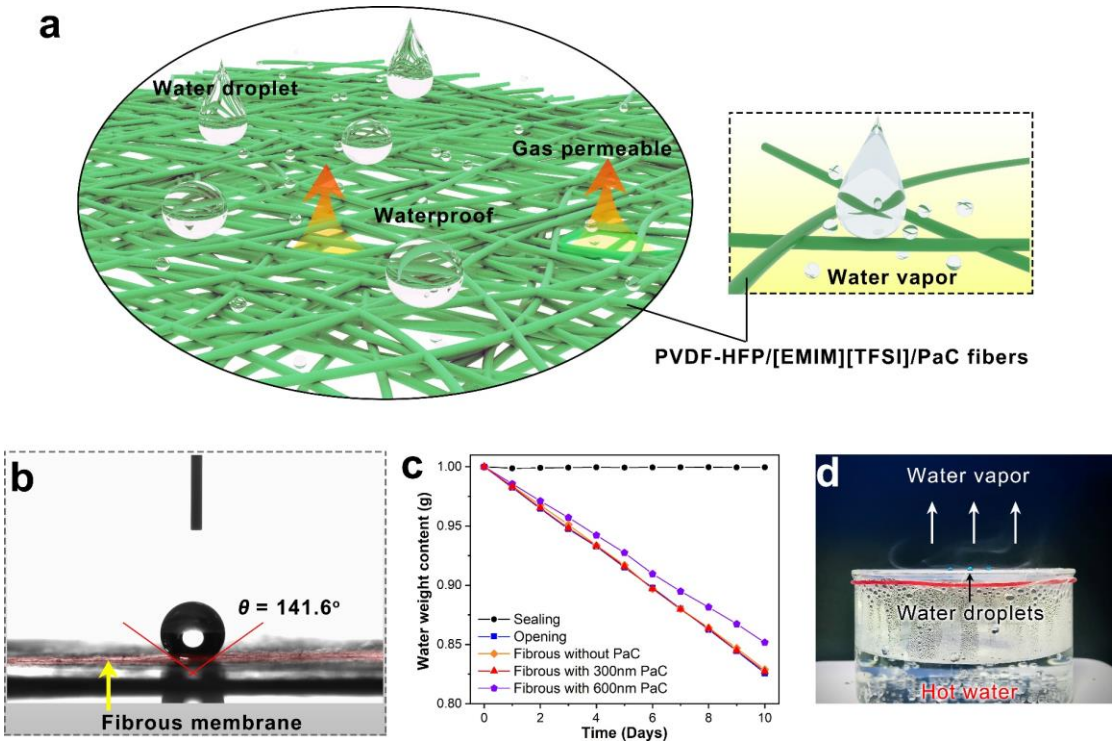


**Figure 2. a** Waterproof and gas-permeable capabilities of fibrous electronics. **b** The contact angle of the fibrous membrane. **c** The comparison of water loss speed for fibrous membrane. **d** Water droplets (dyed with blue ink) were suspended on the hydrophobic surface (Waterproof), and water vapor was

freely passing through the fibrous membrane (Breathable).

**Breathability and waterproof ability.** The breathability of fibrous membrane principally came from the Fickian diffusion of water vapor within the interconnected porous structure of fibrous membranes. The pore size of fibrous is mainly distributed in a range of 10-20 um (Supplementary Fig. S7), which is between the diameters of ultra-fine atomized water vapor (<10 um) and coarse aerosol water droplet (>100 um). The difference of relative humidity drives the water vapor passing through from one side to another side, resulting in gas permeable behaviors. In addition, the hydrophobicity of fluorine-containing PVDF-HFP/[EMIM][TFSI] fibers enhanced the waterproof behaviors of fibrous electrolyte, which was evaluated by measuring the contact angle. **Fig. 2b** indicated a water contact angle of 141.6°, displaying excellent hydrophobicity.

The gas permeability enables gas molecules to pass through the fabric, making it be breathable as on-skin electronics, so that sweat can evaporate through it freely. To evaluate its gas permeability, the weight loss of water in a bottle before and after covering with fibrous membrane was measured. As shown in **Fig. 2c**, a negligible difference in water evaporation rate was obtained after 300 nm PaC coating, which is almost the same as that under no covering, demonstrating a high degree of gas permeability. To further demonstrate the breathable and waterproof behaviors, a beaker containing hot water was covered by our fibrous electrolyte. As shown in **Fig. 2d**, the small water droplets (dyed with Prussian blue for better visualization, 2mm in diameter) can be observed, which were suspended on the hydrophobic surface. Meanwhile, a large amount of water vapor could freely go across the fibrous electrolyte without restrictions. The excellent gas permeability indicates a promising application in wearable electronics for long-term operation.

Next, the phase composition of fibers and films was analyzed by FT-IR spectroscopy (Supplementary Fig. S8). For both pure PVDF-HFP and PVDF-HFP after doping with ionic liquid, the peaks of polar β-phase (1275 $cm^{-1}$) and

electroactive phase at 841 $cm^{-1}$ are more prominent in electrospun fibers than that in films. Meanwhile, the peaks of non-polar α-phase at 764 $cm^{-1}$ and semi-polar γ-phase at 1234 $cm^{-1}$ dominate more in film than that in electrospun fibers. The typical peaks at 1134 $cm^{-1}$ and 1349 $cm^{-1}$ correspond to the vibrational bands of [EMIM][TFSI], indicating the incorporation of the ionic liquid in a polymer matrix. The incorporation of IL results in reducing the peak intensity of the non-polar α-phase in both electrospun fibers and films. These results indicated the prominent phase transformation from α-phase to β-phase after the electrospinning process, which can contribute more to the ionic transport.[40, 41]

The ionic conductivity was also investigated to confirm the enhanced ionic transport in polymer fibers. As shown in Supplementary Fig. S9, the conductivity of fibrous electrolyte ($5.3\times10^{-5}$ S $cm^{-1}$) is determined to be more than 5 times higher than that in film electrolyte ($1.0\times10^{-5}$ S $cm^{-1}$); at the same ionic concentration and without regard to the porosity of fibrous electrolyte. Our result is also in accordance with previous reports that the fibrous and porous polymer electrolyte can enable faster ion mobility[40] and promotes better interfacial contact with the polymer channel for better ion uptake and electrochemical performance.[41] Benefiting from the enhanced ionic conductivity, we fabricated OECTs on fibrous electrolyte.

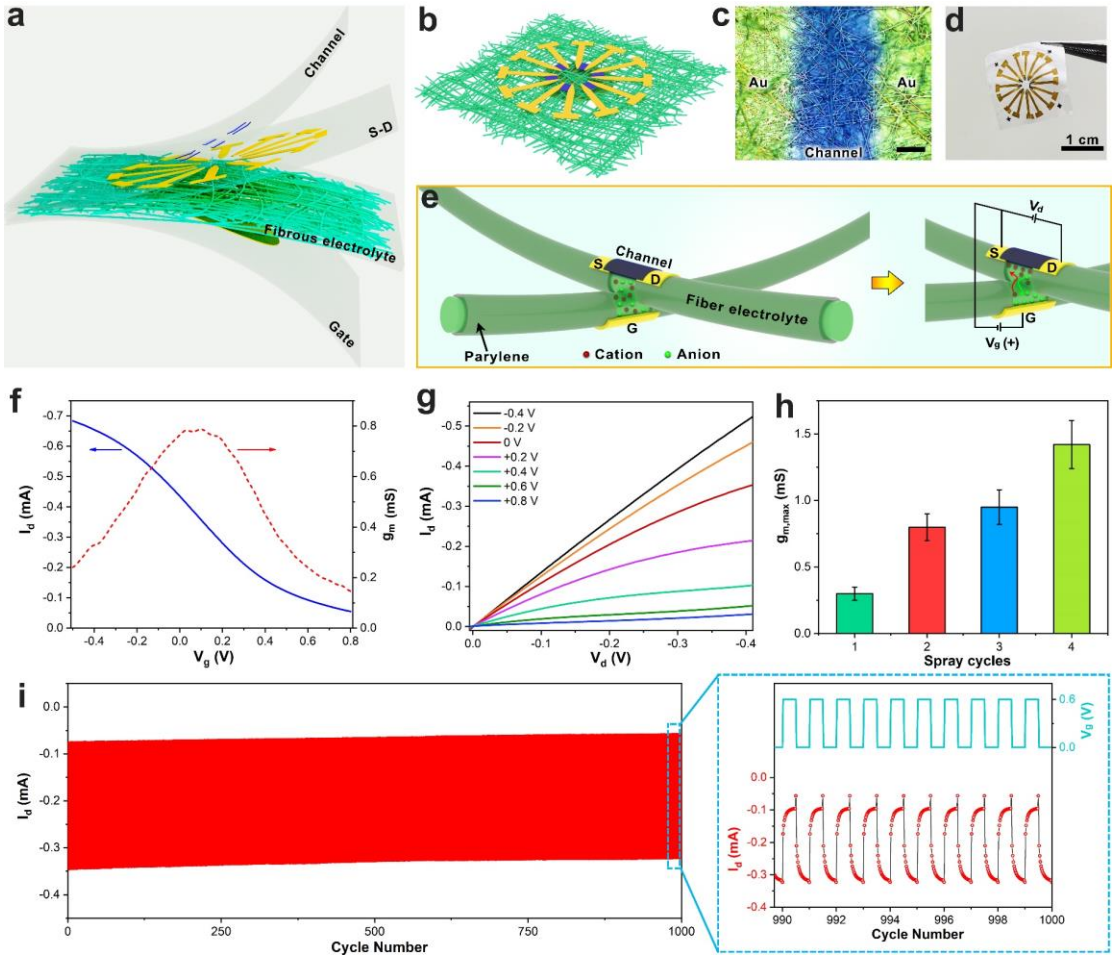


**Figure 3. Fibrous OECT. a-b** The schematic diagram of fibrous OECT. **c** Optical image of the active channel area. (Scale bar: 100 um) **d** Photograph of fibrous OECT. **e** The ionic migration between fiber electrolytes for the doping/dedoping process. **f** Transfer and transconductance curves of fibrous OECT with two spray-printing cycles. (L=200 um, W=1000 um, d=330 nm) **g** Output curve of fibrous OECT. **h** The relationship between maximum transconductance and spray cycles. **i** Pulse measurements with over 1000 cycles of continuous operation for the fibrous OECT ($V_g$ varies from 0 to +0.6 V, pulse width= 0.5 s, $V_d$= -0.5 V). The right image is the transient response of drain current to gate pulse after 1000 cycles.

**Fabrication of fibrous OECTs.** The fibrous OECT was fabricated layer by layer, in which the e-spun fibers serve as the substrate and ionic source simultaneously, as shown in **Fig. 3a-b**. In brief, a shadow mask was used for the Ni/Au (10/60 nm) evaporation on the fabricated fibrous electrolyte substrate, serving as the drain and source electrodes of OECT (Supplementary Fig. S10). The channel length (L) was

varied from 100 um to 250 um, and the channel width (W) was 1000 um. Then reactive ion etching (RIE) process was applied to remove the parylene covered in the active channel area through shadow mask alignment. PEDOT:PSS as the active materials was spray-printed between the S-D electrodes with a shadow mask for patterning (**Fig. 3c**). The thickness of PEDOT:PSS was controlled by repeated spray cycles, where 25 ul/cm$^2$ was defined as one spray cycle (Supplementary Fig. S11a). Next, another Ni/Au (10/60 nm) layer was evaporated on the backside around the center of the fibrous device, working as the bottom gate electrode. The bottom gate configuration of fibrous OECT enables an effective electric field between gate and active materials to actuate the ionic migration. **Fig. 3d** presents the fabricated fibrous OECT with a total thickness of less than 10 um. The details to fabricate fibrous OECT was discussed in the Method section.

In the fibrous electrolyte, there is a high chain dipole moment of PVDF-HFP copolymer interacted with ionic liquid ([EMIM][TFSI]), that allows for facile ion migration along the highly ion-conducting copolymer under applied electric field. As shown in **Fig. 3e**, cations (EMIM+) and anions (TFSI-) can migrate along the fiber electrolyte and across between fiber electrolyte after applying gate bias for the doping/dedoping process in PEDOT:PSS film. The positive gate bias can induce the injection of EMIM+ cations from fibers electrolyte into PEDOT:PSS, which compensates the sulfonate anions of PSS, then the conducting PEDOT will be reduced to the neutral state. In contrast, a negative gate bias results in a dedoping process of EMIM+ in PEDOT:PSS, and more holes will be generated in PEDOT conjugated chain, enabling a highly conducting state of PEDOT.[42]

The transfer ($I_d$-$V_g$) and output ($I_d$-$V_d$) characteristics of fibrous OECT (**Fig. 3f-g**) exhibited a decrease in drain current ($I_d$) upon applying positive gate bias ($V_g$), consistent with the doping process of EMIM+ cations in PEDOT:PSS. The fibrous OECT showed typical p-type depletion mode behaviour as well as other conventional PEDOT:PSS-based OECTs.[42-44] The peak transconductance ($g_m=\Delta I_d/\Delta V_g$) of ~ 0.8 mS was obtained at $V_g$= 0.1V for fibrous OECT with channel dimension of W/L/d=

1000 um/200 um/ 330 nm, comparable to other liquid based OECTs (0.38-0.88 mS) on fibre substrates[45]. In addition, repeating spray cycles could stack thicker PEDOT:PSS and help to fill more pores and bridge more continuous pathways in the channel (Supplementary Fig. S12). Therefore, $g_m$ of OECT increased proportionally with respect to the repeated spray cycles (**Fig. 3h**), and the thickness-normalized $g_m$ was 16.6±4.2 S $cm^{-1}$ (Supplementary Fig. S11b). The large $g_m$ and low voltage operation demonstrated great potential for fibrous OECT working as ideal ion-to-electron transducers. OECT with two spray cycles was chosen for the following experiments if there is no special mention.

The switching stability was performed by continuously applying gate pulse from 0 V to 0.6 V with a duration of 0.5s. **Fig. 3i** indicated that the $I_d$ retained ~90% of its initial value after 1000 cycles, demonstrating an excellent stability of fibrous OECT and well suited for the long-term operation.

Supplementary Fig. S13 exhibited the temporal response of $I_d$ to a gate pulse with 1s duration and 0.6 V amplitude at constant $V_d$= -0.5 V. The rise time largely depends on the thickness of PEDOT:PSS, and a rise time of 0.06 s for fibrous OECT with one spray cycle (*d= 180 nm*) was obtained by exponential decay fitting the $I_d$ variation. OECT based on film electrolyte exhibited a much slower transient response (0.22s) due to the less polar β-phase and lower ionic conductivity of film electrolyte. The fast temporal response and high $g_m$ enable our fibrous OECT to monitor the bio-electrophysiological signals.

Ionic concentration within electrolytes has a great influence on OECT performance. We optimized the ionic concentration of $W_{PVDF\text{-}HFP}$:$W_{IL}$ from 4:1 to 1:4 and compared the basic transfer characteristics (Supplementary Fig. S14). There is no ionic doping process in PEDOT:PSS while using pure PVDF-HFP fibers. With the increasing IL content, on current at $V_g$= -0.4V is also increasing due to the morphology tuning induced by IL[42], and the leakage current ($I_{gs}$) is increasing due to the improved ionic conductivity. Fibrous electrolyte with higher ionic concentration ($W_{PVDF\text{-}HFP}$:$W_{IL}$ = 1:4) was prepared for OECTs. The OECT presented a higher $g_m$ (1.2 mS), faster transient

response (τ=16 ms), and good switching stability over 1000 cycles (~88% performance retention) (Supplementary Fig. S15).

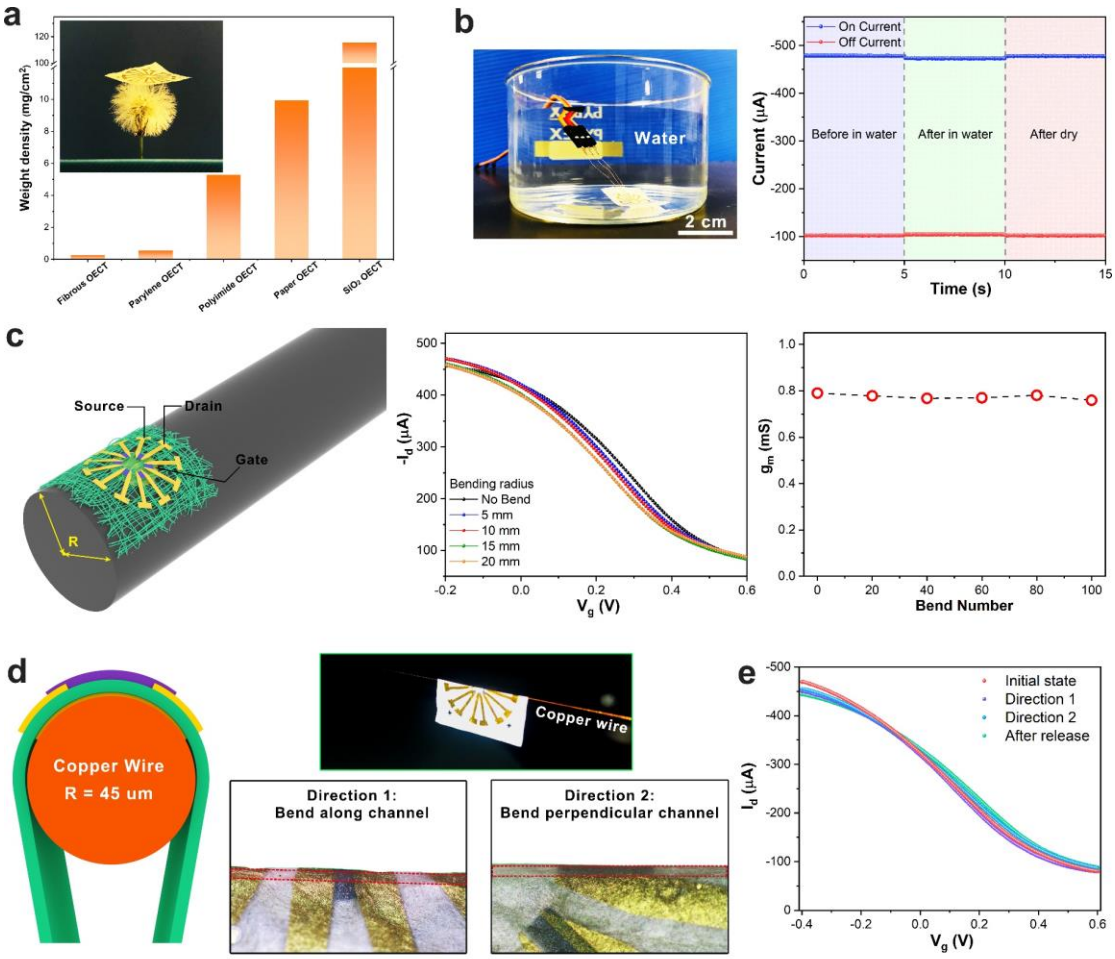


**Figure 4. The lightweight, waterproof and bending-insensitive behaviors and of Fibrous OECT. a** The weight of OECT devices fabricated on different substrates (Fibrous, parylene, polyimide, paper, silicon wafer). The inset image shows the placement of a fibrous OECT on a dandelion to demonstrate its lightweight. **b** The waterproof ability of fibrous OECT. The left image is an optical image of fibrous OECT wholly submerged in DI water and its on/off current signals recorded before and after submerged in DI water, and after being fully dried in an oven, indicating the excellent stability against water. **c** The bending stability of fibrous OECT. The transfer characteristics of OECT under different bent states and the maximum $g_m$ at different bend numbers were measured. **d** Schematic representation of fibrous OECTs wrapped around a copper wire. The bottom right photos present different wrapping states, bending along or perpendicular to channel length directions. **e** Transfer characteristics of fibrous

OECT under different wrapping states around a copper wire.

**Lightweight, waterproof and bending-insensitive behaviors and of Fibrous OECT.** Benefitting from the ultrathin porous structure and hydrophobic materials, our fibrous OECT showed super lightweight, waterproof and excellent flexibility. In addition, the e-spinning and spray-printing technologies enable the facial fabrication of imperceptible electronic devices with only micro-scale total thickness, thus minimizing electronic waste. The porous structure in fibrous membrane can substantially reduce the mass loading as an epidermal electronic. Compared with other OECTs fabricated on various substrates, our fibrous OECT is only 0.25 mg/cm$^2$, which is 20-fold lighter than OECT on polyimide substrates (26.3 um thick, 5.3 mg/cm$^2$), 39-fold lighter than OECT on office paper (102.3 um thick, 9.9 mg/cm$^2$) and 450-fold lighter than OECT on the conventional silicon wafer substrate (508.2 um, 116 mg/cm$^2$) (Supplementary Fig. S16). An example to show its lightweight is shown in **Fig. 4a**, in which the final fibrous OECT device can stand on top of a dandelion without even bending the flower's seed.

Waterproof ability enables the fibrous OECT to operate well in water. As shown in **Fig. 4b**, the fibrous OECT was wholly submerged in DI water during the measurement. The on/off current presented negligible signal variation before and after being submerged in water, and the slight fluctuation mainly resulted from the increase of leakage current after putting in water. After being fully dried in an oven, unchanged signals were observed (Supplementary Fig. S17).

The durability of fibrous OECT over time was also investigated. As shown in Supplementary Fig. S18, the device stored in air for over one month showed slight decline of 80% retention in performance, proving its long-term durability.

To explore its flexibility, the fibrous OECT was bent with a bending radius from 5 mm to 20 mm. The bending radius was defined as shown in **Fig. 4c**. The transfer characteristics remained unaffected before and after the bend deformation, thanks to the excellent softness and flexibility. In addition, after 100 times repeated bending,

almost 95% transconductance was maintained, proving its robustness and bending-insensitivity. The bending insensitivity was comparable to the fabric OECTs fabricated on Nylon fibers, which present stable performance at different bending radius and repeated bending times.[17] Benefiting from the bending insensitivity, our fibrous OECT was hung on a copper wire with a radius of 45 um (Supplementary Fig. S19), and the changes in performance were found to be negligibly small before and after wrapping along or perpendicular to channel directions (**Fig. 4d-e**). Fibrous OECT on human skin exhibited comparable performance with that in normal conditions, proving a great potential as on-skin electronics (Supplementary Fig. S20). As a result, the fibrous OECT shows excellent softness, waterproofness, and robustness, satisfying the requirements for comfortable and reliable on-skin electronics. Taking advantage of these superiorities, our fibrous OECT can also be well adapted to some extreme environments, such as swimming or exercising, and therefore be used in wearable sports, healthcare, and biomedical systems.

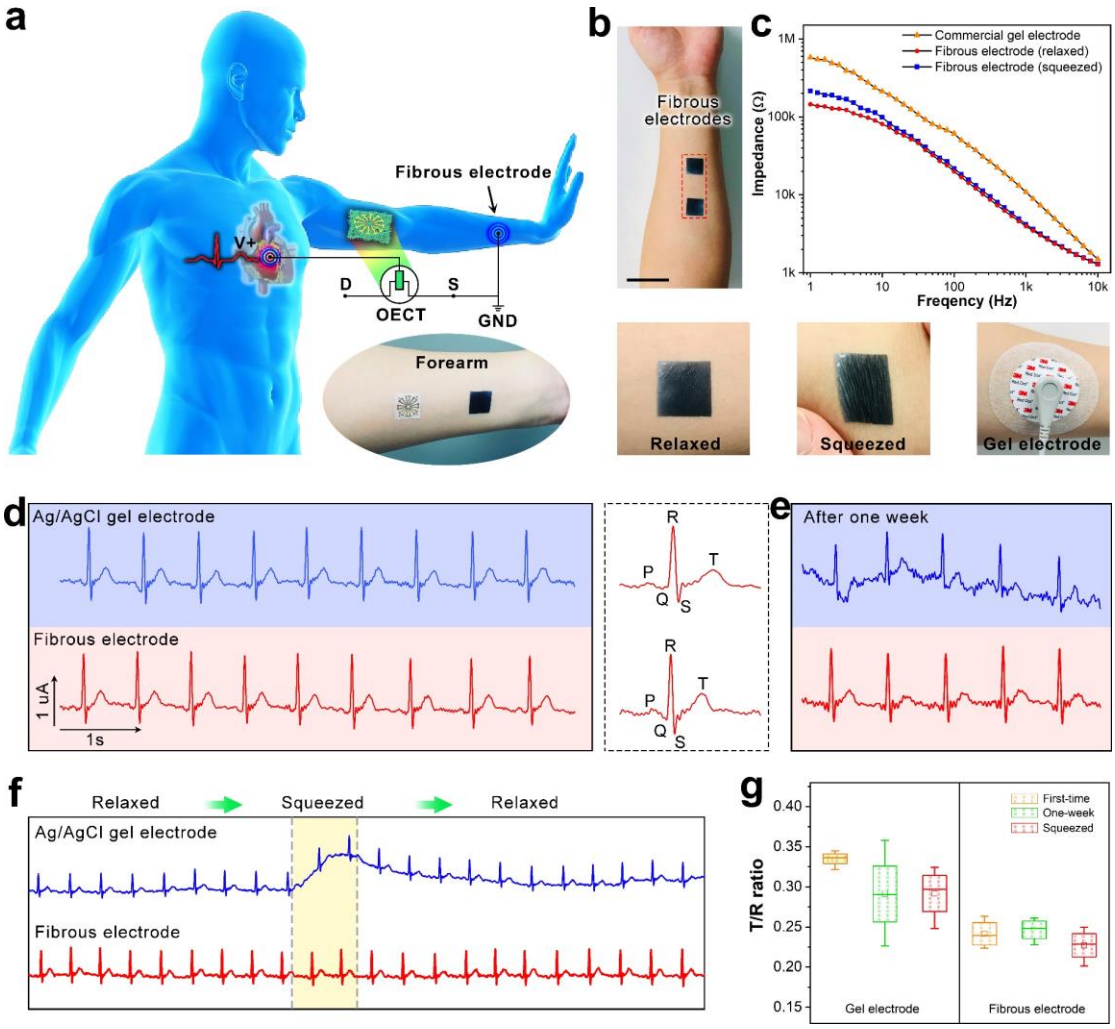


**Figure 5. Electrocardiography (ECG) monitoring using fibrous electrodes and OECT. a** Schematic illustration of the ECG monitoring. The bottom right image is the adhesion of fibrous OECT and electrode on the human forearm as on-skin electronics. **b** Photos of fibrous electrodes fabricated by spray-coating PEDOT:PSS/eg solution on fibrous substrate. The electrodes were placed onto the volunteer's forearm with a center-to-center distance of 5 cm. The electrodes could attach firmly to the skin and deformed freely with squeezed. Commercial gel electrodes were used to compare the ECG measurement. **c** Impedance spectra of commercial Ag/AgCl gel electrode and fibrous electrodes on the skin. **d** Comparison of ECG signals using a commercial gel electrode and fibrous electrode. The left image is a detailed view of the recording. **e** ECG signal using some electrodes after one week. **f** ECG testing on the skin while squeezing the skin. **g** The T/R peak ratio of ECG signals for commercial gel electrode and fibrous electrode under different recording conditions.

**Electrocardiography monitoring using fibrous electrodes and OECT.** To explore the application of fibrous OECT, ECG signals were collected on human skin with fibrous electrodes (**Fig. 5a**). As known, the potential amplitudes generated by body activities distribute in a range from tens of microvolt to tens of millivolt.[13] ECG, as the main technique to record cardiac activity, can provide useful information about the

normal function or abnormalities of the heart.[46] The potential (~1 mV) is generated from the depolarization of the ventricles. OECT is a good signal amplifier, holding the advantages such as high signal-to-noise ratio, high transconductance, and low operating voltage, allowing OECT to monitor ECG signals even at a very low level of gate bias (Supplementary Fig. S21). In addition, the fibrous OECT is biocompatible, flexible, and soft, allowing OECT to be loaded on the target surface of human skin and withstand external deformations.

To fabricate the fibrous electrode for ECG testing, PEDOT:PSS was spray-coated on the fibrous substrate, which acted as a support scaffold. The fibrous electrode is soft, waterproof, gas permeable, and robust, which will adhere to the skin with the help of a bit of water. **Fig. 5b** shows images of the fibrous electrodes after being transferred on the human forearm, demonstrating a conformal contact with human skin. Such tight (intimate) and conformal bonding to the skin ensures the stability to withstand the external squeeze deformation, presenting promise for use as biomedical electrode. Compared to commercial gel electrodes, the fibrous electrodes show a contact impedance over 60% lower than that obtained from commercial gel electrodes with the same contact area (~2.5 $cm^2$) over frequencies ranging from 1 to 10 kHz (**Fig. 5c**). In addition, the impedance shows a negligible variation while squeezing the skin. The reason comes from the excellent conductivity and conformability of the fibrous, which enhanced the intimate bonding to skin and decreased the bending stiffness.

Both the gel and fibrous electrodes were used as on-skin electrodes to obtain ECG signals. In the measurement, one electrode was adhered to the volunteer's chest and connected to the gate electrode of fibrous OECT, while another electrode was adhered to the left forearm and connected to the source electrode of fibrous OECT. A drain bias of -0.5 V was applied to record the channel current in both relaxed and squeezed states. As shown in **Fig. 5d**, the ECG signals acquired by the gel and fibrous electrodes turned out to be comparable while the skin was in a relaxed condition. In both cases, the recorded traces, including P-wave, T-wave, and QRS complex, corresponding to the expected electrical activity of a human heart could be recognized

clearly, demonstrating a reliable ECG signal was collected. The potential generated by cardiac activity was transmitted to the current signal by fibrous OECT with a peak-to-peak amplitude of around 1 uA. The signal-to-noise ratio (SNR) in ECG signals was calculated to be 21.7 dB for OECT with fibrous electrode and 22.91 dB for OECT with gel electrode, indicating a comparable high-quality signal without any external amplifying circuits. However, the fibrous electrodes could be used for long-term healthcare monitoring, without noticeable fluctuations of the ECG signal even after one week, while the commercial gel electrodes showed remarkable peak fluctuations and baseline drift over time (**Fig. 5e**). The reason comes from the non-degraded adhesiveness on skin and conductivity to collect effective skin potential for the dry fibrous electrode, and non-adhesive attaching on skin and water loss for gel electrodes.

Another superiority of fibrous on-skin electronics is its conformal stability even when the skin deformed significantly, such as in the case of skin squeezing. As shown in **Fig. 5f**, if the skin squeezed during the signal recording, the ECG signal collected by fibrous electrodes remained unaffected, and negligible noise and fluctuation in the baseline were obtained, owing to the negligible delamination and low skin-electrode impedance under the skin deformation. In contrast, the signal acquired from gel electrodes presented a clear baseline drift and unidentifiable features, due to the occurrence of non-conformal contact surface during skin squeezing.

To clearly compare the signal fluctuation, we analyzed the T/R ratio in ECG signals over time and skin squeezing. **Fig. 5g** shows the comparable signal quality for both fresh gel and fibrous electrodes where the T/R ratio is distributed in a narrow range. During the skin squeezing measurement or over one week, large fluctuations of the T/R ratio were obtained for gel electrodes, while only minor fluctuations for fibrous electrodes. As a result, the conformal and stable fibrous on-skin device is well suited to acquire high quality ECG signals and shows great potential for other electrophysiological signals as epidermal electronics.

**Discussion**

In this paper, a lightweight, waterproof and breathable fibrous OECT was developed for on-skin electronics. The fibrous network possessed high mechanical robustness and excellent waterproofness, gas permeability. The fibrous OECTs were demonstrated with transconductance from 0.25 mS to 1.60 mS, which could be modulated by spray coating cycles. The stability measurements indicated a performance retention of above 90% after ~1000 operating cycles or 30 days after being kept in air condition. The light weight (0.25 mg/cm$^2$), waterproof behaviors, and insusceptible to bending deformation for fibrous OECT demonstrated its well suitable for on-skin electronics as a local signal amplifier to convert tiny voltage signals. For the first time, our all-in-one fibrous OECT was used to record ECG signals by combining the fibrous electrode on the skin to collect the potential generated by cardiac activity. The conformal contact on human skin and signal amplification function of fibrous OECT enable a high-quality ECG signal with minor fluctuation and stable recording over time (one week) and skin squeezing, paving the way for other electrophysiological signals as epidermal electronics. In addition, the industrial manufacturing is foreseeable to produce large-area fibrous electronics, providing a cost-effective production for the application in emerging soft textile electronics.

## Methods

***Materials:*** Poly(3,4-ethylenedioxythiophene):poly(styrenesulfonate) (PEDOT:PSS, Clevios PH1000) were purchased from Heraeus. Poly(vinylidene fluoride-co-hexafluoropropylene) (PVDF-co-HFP, Mw= 400,000 g/mol), ethylene glycol (eg), 1-Ethyl-3-methylimidazolium bis(trifluoromethylsulfonyl)amide ([EMIM][TFSI]), (3-glycidyloxypropyl)trimethoxysilane (GOPS) were purchased from Sigma-Aldrich and used as received.

**Synthesis of fibrous electrolyte:** Precursor solution for electrospinning was prepared by mixing PVDF-HFP, EMIM:TFSI and DMF with a weight ratio of 1:1:10. Stirring and heating at 70 ºC were performed until the solution was transparent and uniform. Electrospinning machine (Elite, Beijing Ucalery Technology Development Co., Ltd) was used to fabricate fiber electrolyte with a distance of 20 cm between the syringe needle and collector. During the electrospinning, high DC voltage of +15 kV and -5.0 kV were applied on the syringe needle and collector, respectively. The feed rate was controlled to be 30 ul/min. Then 300 nm parylene C was coated on the fibrous electrolyte by chemical vapor deposition (Lavida-110, Femto Science Inc) to enhance the junction between fibers. Shadow mask was used to pattern Ni/Au (10 nm/60 nm) electrode on the parylene-coated fibrous electrolyte.

**Fabrication of fibrous OECTs:** The channel of OECT was exposed via etching the parylene layer using $O_2$ plasma RIE process. The etching time (150s with an etching speed of 2 nm/s) was optimized to ensure the integrity of fiber electrolyte and fully remove the parylene C in channel area. A shadow mask was used to pattern the channel area with dimension (W×L) of (100-250) μm × 1000 μm. PEDOT:PSS solution was prepared by mixing pristine PEDOT:PSS aqueous solution (1ml), ethylene glycol (0.05ml), DI water (1ml) and GOPS (5μl). The solution was used for spray coating as active materials of OECT via a commercial spray coating system. The nozzle was controlled with a moving speed of 10 cm/s and height of around 15 cm. The substrate was fixed on the hotplate and kept a temperature of 90 ºC for the fast evaporation of solvent. Shadow mask was used for the patterning of channel area

during the spray coating process and the thickness of PEDOT:PSS could be controlled by different cycles of spray coating. Here one cycle was defined as 1ml solution spray coating for 4cm × 10cm area (i.e. 25 ul/cm$^2$). After the spray coating, the film was annealed at 120 ºC for 20 min. Next, the gate electrode (Ni/Au, 10 nm/60 nm) was deposited on the back side of fibrous electrolyte.

**Sheet resistance Measurement:** The samples were prepared by spray coating PEDOT:PSS (5 cycles) and depositing Ni/Au (10 nm/60 nm) on the fibrous substrate after coating parylene. The sheet resistances of Au and PEDOT:PSS on fibrous substrates were measured by the four-point probe system (Ossila Ltd). Data were collected from four samples.

**Mechanical Testing:** The successive mechanical deformation was conducted using a highly configurable tensile tester (ESM-303, Mark-10 Corporation) with a force gauge (Mark-10 025/012). The stress-strain behaviors were measured by stretching the samples with a fixed speed of 20 mm/min. All measurements were repeated for 3 times at ambient temperature. The poking measurement was performed using a pipette, which was mounted on the force gauge and applying force on the fibrous substrate. The stress was recorded in the real-time during the poking process.

**Measurement of water vapor permeability:** The water vapor permeability was conducted by measuring the weight loss of water permeated through the fibrous membrane. Firstly, 1 g of DI water was placed in a 1.5ml glass bottle with an opening aperture (0.5cm in diameter). Then, the glass bottle was covered with our fibrous membrane (Fibrous with 300nm PaC). Control groups were conducted by covering no fibrous membrane (Opening), covering its original cap (Sealing) and fibrous membrane with 200 nm PaC. The bottle was placed in air condition with temperature around 25 ºC and 30% humidity for ten days. Then the weight loss of the water was measured day by day.

**Stability measurement:** For measurement of waterproof stability, fibrous OECT was immersed into DI water and recorded the variation of electrical signals. For long-term stability measurement, fibrous OECT was stored in air condition until 30 days.

**Contact impedance measurement:** The fibrous electrode was prepared by spray coating PEDOT:PSS solutions on the fibrous substrate. Then, the fibrous electrode was cut into fibrous pieces with size of 1.6 cm × 1.6 cm. Pairs of fibrous pieces were placed onto the skin of left forearm with a center-to-center distance of 5 cm after slightly wetting with few DI water. The electrode-skin contact impedance was measured using an electrochemical analyzer (Metrohm Autolab PGSTAT302N) over a frequency range from 1 to 10 kHz in both relaxed state and squeezed state. For the comparison, gel electrode (3M Red Dot ECG monitoring electrodes, 2248-50, diameter of gel area is ~1.8 cm) was placed on skin of left forearm with same center-to-center distance. All the measurement parameters are as same as that of fibrous electrodes.

**Ionic conductivity measurement:** The real part of the impedance and phase angle for all samples were measured using an electrochemical analyzer (Metrohm Autolab PGSTAT302N). An AC voltage of 10 mV was applied while sweeping the frequency from 1MHz to 1Hz. The measurement was implemented at room temperature. A coin cell was used to perform the ionic conductivity measurement. The electrolyte was sandwiched between two stainless-steels discs (diameter of 1.6cm, used as electrodes). The ionic conductivity is calculated using the equation: $\sigma = L/(A \times R_b)$, where $R_b$ is bulk resistance, taken at the frequency when the phase angle is closest to 0, L is the distance between the two stainless steels, and A is the area of stainless steel.

**ECG signals measurement:** Both the commercial gel and fibrous electrodes were used as on-skin electrodes to obtain ECG signals. In the measurement, one electrode was adhered to the volunteer's chest and connected to the gate electrode of fibrous OECT, while another electrode was adhered to the left forearm and connected to the source electrode of fibrous OECT. A drain bias of -0.5 V was applied to record the channel current in both relaxed and squeezed states. The ECG signal was recorded by a Keysight precision source/measure unit (B2912A). SNR of ECG signals was calculated from the following equation, $SNR_{dB}=20\log_{10}(A_{signal}/A_{noise})$, where $A_{signal}$ is the RMS of the ECG signals and $A_{noise}$ is the RMS of the noise collected at zero input

potential (ST segment in ECG signal). The measurements were approved by Institutional Review Board at Nanyang Technological University (Approval number: IRB-2021-144).

**Device Characterization:** The metal electrodes were deposited by Thermal evaporator system (Solar-Passage, Daedong high Technologies). The SEM morphology was measured using field emission scanning electron microscopy (FE-SEM, JEOL, JSM-7600F). The contact angle was tested by OCA15Pro (Dataphysics). The transistor behaviors measurements were carried out using a Keithley 1500 semiconductor analyzer. The mechanical properties were carried out by a tensile tester (ESM-303, Mark-10 Corporation).

## Author Contributions:

The manuscript was written through contributions of all authors. Chen. S and Leong WL conceived the idea, designed the experiment. Chen S and Wang Z fabricated the fibrous membrane. Chen S collected and analyzed data. Hou KQ performed the SEM measurements. Li T performed the contact angle and FT-IR measurements. Wu XH performed the coating of parylene C and the thickness measurement for conducting polymers. Wei L and Leong. WL supervised the project.

## Acknowledgements

This research was supported primarily by Ministry of Education (MOE) under AcRF Tier 2 grant (2019-T2-2-106) and National Robotics Programme (W1925d0106).

## Competing interests

The authors declare no competing interests.

## Data availability

The source data underlying the figures in the main manuscript and Supplementary Information are provided as Source Data file. All other data that support the findings of this study are available from the corresponding authors upon reasonable request. Source data are provided with this paper.

**References**


[1] J. Lv, G. Thangavel, Y. Li, J. Xiong, D. Gao, J. Ciou, M. W. M. Tan, I. Aziz, S. Chen, J. Chen, X. Zhou, W. C. Poh, P. S. Lee, *Sci. Adv.* **2021**, *7*, eabg8433.

[2] C. Tan, Z. Dong, Y. Li, H. Zhao, X. Huang, Z. Zhou, J. W. Jiang, Y. Z. Long, P. Jiang, T. Y. Zhang, B. Sun, *Nat. Commun.* **2020**, *11*, 3530.

[3] W. Gao, S. Emaminejad, H. Y. Y. Nyein, S. Challa, K. Chen, A. Peck, H. M. Fahad, H. Ota, H. Shiraki, D. Kiriya, D. H. Lien, G. A. Brooks, R. W. Davis, A. Javey, *Nature* **2016**, *529*, 509.

[4] Y. J. Fan, X. Li, S. Y. Kuang, L. Zhang, Y. H. Chen, L. Liu, K. Zhang, S. W. Ma, F. Liang, T. Wu, Z. L. Wang, G. Zhu, *ACS Nano* **2018**, *12*, 9326.

[5] X. Peng, K. Dong, C. Ye, Y. Jiang, S. Zhai, R. Cheng, D. Liu, X. Gao, J. Wang, Z. L. Wang, *Science Advances* **2020**, *6*, eaba9624.

[6] H. Jinno, K. Fukuda, X. Xu, S. Park, Y. Suzuki, M. Koizumi, T. Yokota, I. Osaka, K. Takimiya, T. Someya, *Nature Energy* **2017**, *2*, 780.

[7] A. Miyamoto, S. Lee, N. F. Cooray, S. Lee, M. Mori, N. Matsuhisa, H. Jin, L. Yoda, T. Yokota, A. Itoh, M. Sekino, H. Kawasaki, T. Ebihara, M. Amagai, T. Someya, *Nat. Nanotechnol.* **2017**, *12*, 907.

[8] S. Lee, S. Franklin, F. A. Hassani, T. Yokota, M. O. G. Nayeem, Y. Wang, R. Leib, G. Cheng, D. W. Franklin, T. Someya, *Science* **2020**, *370*, 966.

[9] J. Xiong, P. Cui, X. Chen, J. Wang, K. Parida, M. F. Lin, P. S. Lee, *Nat. Commun.* **2018**, *9*, 4280.

[10] X. Tian, P. M. Lee, Y. J. Tan, T. L. Y. Wu, H. Yao, M. Zhang, Z. Li, K. A. Ng, B. C. K. Tee, J. S. Ho, *Nature Electronics* **2019**, *2*, 243.

[11] W. Zeng, L. Shu, Q. Li, S. Chen, F. Wang, X. M. Tao, *Adv. Mater.* **2014**, *26*, 5310.

[12] J. Rivnay, S. Inal, A. Salleo, R. M. Owens, M. Berggren, G. G. Malliaras, *Nature Reviews Materials* **2018**, *3*, 17086.

[13] S. Chen, A. Surendran, X. Wu, S. Y. Lee, M. Stephen, W. L. Leong, *Advanced Materials Technologies* **2020**, *5*, 2000523.

[14] A. Nawaz, Q. Liu, W. L. Leong, K. E. Fairfull-Smith, P. Sonar, *Adv. Mater.* **2021**, e2101874.

[15] N. Wang, A. Yang, Y. Fu, Y. Li, F. Yan, *Acc. Chem. Res.* **2019**, *52*, 277.

[16] H. Liu, A. Yang, J. Song, N. Wang, P. Lam, Y. Li, H. K. Law, F. Yan, *Sci. Adv.* **2021**, *7*, eabg8387.

[17] A. Yang, Y. Li, C. Yang, Y. Fu, N. Wang, L. Li, F. Yan, *Adv. Mater.* **2018**, *30*, 1800051.

[18] C. Cea, G. D. Spyropoulos, P. Jastrzebska-Perfect, J. J. Ferrero, J. N. Gelinas, D. Khodagholy, *Nat. Mater.* **2020**, *19*, 679.

[19] P. Leleux, J. Rivnay, T. Lonjaret, J. M. Badier, C. Benar, T. Herve, P. Chauvel, G. G. Malliaras, *Adv. Healthc. Mater.* **2015**, *4*, 142.

[20] P. Jastrzebska-Perfect, G. D. Spyropoulos, C. Cea, Z. Zhao, O. J. Rauhala, A. Viswanathan, S. A. Sheth, J. N. Gelinas, D. Khodagholy, *Science Advances* **2020**, *6*, eaaz6767.

[21] A. Savva, C. Cendra, A. Giugni, B. Torre, J. Surgailis, D. Ohayon, A. Giovannitti, I. McCulloch, E. Di Fabrizio, A. Salleo, J. Rivnay, S. Inal, *Chemistry of Materials* **2019**, *31*, 927.

[22] S. M. Kim, C. H. Kim, Y. Kim, N. Kim, W. J. Lee, E. H. Lee, D. Kim, S. Park, K. Lee, J. Rivnay, M. H. Yoon, *Nature Communications* **2018**, *9*, 3858.

[23] G. D. Spyropoulos, J. N. Gelinas, D. Khodagholy, *Science Advances* **2019**, *5*, eaau7378.

[24] D. Khodagholy, V. F. Curto, K. J. Fraser, M. Gurfinkel, R. Byrne, D. Diamond, G. G. Malliaras, F. Benito-Lopez, R. M. Owens, *Journal of Materials Chemistry* **2012**, *22*, 4440.

[25] Y. Na, F. S. Kim, *Chemistry of Materials* **2019**, *31*, 4759.

[26] C. G. Bischak, L. Q. Flagg, D. S. Ginger, *Advanced Materials* **2020**, 2002610.

[27] C. Yang, Z. Suo, *Nature Reviews Materials* **2018**, *3*, 125.
[28] L. Shi, T. Zhu, G. Gao, X. Zhang, W. Wei, W. Liu, S. Ding, *Nature Communications* **2018**, *9*, 2630.
[29] H. Yuk, B. Lu, X. Zhao, *Chem. Soc. Rev.* **2019**, *48*, 1642.
[30] H. Lee, S. Lee, W. Lee, T. Yokota, K. Fukuda, T. Someya, *Advanced Functional Materials* **2019**, *29*, 1906982.
[31] B. Nketia-Yawson, S. J. Kang, G. D. Tabi, A. Perinot, M. Caironi, A. Facchetti, Y. Y. Noh, *Adv. Mater.* **2017**, *29*, 1605685.
[32] T. J. Quill, G. LeCroy, A. Melianas, D. Rawlings, Q. Thiburce, R. Sheelamanthula, C. Cheng, Y. Tuchman, S. T. Keene, I. McCulloch, R. A. Segalman, M. L. Chabinyc, A. Salleo, *Advanced Functional Materials* **2021**, *31*, 2104301.
[33] K. H. Lee, M. S. Kang, S. Zhang, Y. Gu, T. P. Lodge, C. D. Frisbie, *Advanced Materials* **2012**, *24*, 4457.
[34] K. Sim, F. Ershad, Y. Zhang, P. Yang, H. Shim, Z. Rao, Y. Lu, A. Thukral, A. Elgalad, Y. Xi, B. Tian, D. A. Taylor, C. Yu, *Nature Electronics* **2020**.
[35] H. Cheng, X. He, Z. Fan, J. Ouyang, *Advanced Energy Materials* **2019**, *9*, 1901085.
[36] D. Zhao, A. Martinelli, A. Willfahrt, T. Fischer, D. Bernin, Z. U. Khan, M. Shahi, J. Brill, M. P. Jonsson, S. Fabiano, X. Crispin, *Nature Communications* **2019**, *10*, 1093.
[37] S. H. Cho, S. W. Lee, S. Yu, H. Kim, S. Chang, D. Kang, I. Hwang, H. S. Kang, B. Jeong, E. H. Kim, S. M. Cho, K. L. Kim, H. Lee, W. Shim, C. Park, *ACS Appl. Mater. Interfaces* **2017**, *9*, 10128.
[38] R. Li, Y. Si, Z. Zhu, Y. Guo, Y. Zhang, N. Pan, G. Sun, T. Pan, *Adv. Mater.* **2017**, *29*, 1700253.
[39] S. Chen, A. Surendran, X. Wu, W. L. Leong, *Advanced Functional Materials* **2020**, *30*, 2006186.
[40] A. Sultana, M. M. Alam, S. Fabiano, X. Crispin, D. Zhao, *Journal of Materials Chemistry A* **2021**, *9*, 22418.
[41] D.-W. Kang, J.-K. Kim, *Journal of Electroanalytical Chemistry* **2016**, *775*, 37.
[42] X. Wu, M. Stephen, T. C. Hidalgo, T. Salim, J. Surgailis, A. Surendran, X. Su, T. Li, S. Inal, W. L. Leong, *Advanced Functional Materials* **2021**, 2108510.
[43] X. Wu, A. Surendran, M. Moser, S. Chen, B. T. Muhammad, I. P. Maria, I. McCulloch, W. L. Leong, *ACS Appl. Mater. Interfaces* **2020**, *12*, 20757.
[44] X. Wu, A. Surendran, J. Ko, O. Filonik, E. M. Herzig, P. Muller-Buschbaum, W. L. Leong, *Adv. Mater.* **2019**, *31*, 1805544.
[45] J. Wang, S. Lee, T. Yokota, Y. Jimbo, Y. Wang, M. O. G. Nayeem, M. Nishinaka, T. Someya, *ACS Applied Electronic Materials* **2020**, *2*, 3601.
[46] L. Zhang, K. S. Kumar, H. He, C. J. Cai, X. He, H. Gao, S. Yue, C. Li, R. C. Seet, H. Ren, J. Ouyang, *Nat. Commun.* **2020**, *11*, 4683.